Special Issue
Martensitic and Bainitic Transformations in Steels; Fundamentals and Their Applications

ISIJ International, Vol. 64 (2024), No. 2, pp. 381–388
https://doi.org/10.2355/isijinternational.ISIJINT-2023-141

# Effect of Bain Unit Size on Low-temperature Fracture Toughness in Medium-carbon Martensitic and Bainitic Steels

Akinobu SHIBATA,[1,2)]* Tomoyuki KATSUNO,[2)] Mizuki TSUBOI[2,3)] and Nobuhiro TSUJI[2)]

1) Research Center for Structural Materials, National Institute for Materials Science, 1-2-1, Sengen, Tsukuba, Ibaraki, 305-0047 Japan.
2) Department of Materials Science and Engineering, Kyoto University, Yoshida-honmachi, Sakyo-ku, Kyoto, 606-8501 Japan.
3) Research Division of Machining & Molding, Osaka Research Institute of Industrial Science and Technology, 2-7-1, Ayumino, Izumi-city, Osaka, 594-1157 Japan.

(*Received April 20, 2023; Accepted June 12, 2023; Advance online published July 3, 2023; Published January 30, 2024*)

This study investigated the low-temperature fracture toughness of martensite and bainite with various Bain unit sizes. The three-point bending tests revealed that the apparent fracture toughness increased with decreasing the Bain unit size. We also found that even when the carbide size and distribution were almost the same, the apparent fracture toughness of tempered martensite with Bain unit size of 2.5 $\mu$m was much higher than that of bainite with Bain unit size of 16.2 $\mu$m. The propagation of micro-crack stopped at the Bain unit boundaries when the Bain unit size was small. The additional load was necessary for further propagation of crack which stopped at the Bain unit boundaries, leading to the improvement of fracture toughness. The critical local fracture toughness corresponding to the propagation of crack across the Bain unit boundaries was estimated at 1.04 MPa $m^{1/2}$ by finite element simulations. Based on this value, we proposed that the Bain unit boundary whose interval was less than 9.4 $\mu$m could become obstacle for the crack propagation after penetrating matrix/carbide boundary.

KEY WORDS: low-temperature embrittlement; fracture toughness; cleavage fracture; bainite; martensite.

## 1. Introduction

High-strength steels, particularly martensitic/bainitic steels, exhibit brittle behavior at low temperature, so-called low-temperature embrittlement.[1,2)] To develop advanced high-strength steels with high resistance to low-temperature embrittlement, understanding the relationship between fracture behavior at low temperature and the microstructure is very important.

The representative microstructures in high-strength steels are lath martensite and bainite. Both microstructures are composed of various structural units, and an austenite grain is divided by lath (bainitic lath), block, and packet.[3–7)] A lath is a single crystal of martensite (or bainite) and contains a high density of dislocations. A block is composed of an aggregation of laths with nearly the same crystallographic orientation, and a packet consists of laths with nearly the same habit plane orientation. Due to the existence of various structural units, martensite and bainite contain several kinds of boundaries, such as lath boundaries, block boundaries, packet boundaries, and prior austenite grain boundaries, whose crystallographic features are different from one another. Except for the lath boundaries whose misorientation is ranging from 1 to 5°,[6)] many of the block, packet, and prior austenite grain boundaries are high-angle boundaries which contribute to the strength of materials. To date, several attempts have been conducted to determine the effective boundary of martensite and bainite for low-temperature embrittlement. Pioneering work by Matsuda *et al.*[8)] showed that the facet size of cleavage fracture had a good correlation with block size in tempered martensitic and bainitic steels. Wang *et al.*[9)] proposed that packet boundaries were the most effective boundaries for low-temperature embrittlement based on the observation results that the cleavage crack propagation was deflected at the packet boundaries in a low-carbon martensitic steel. Takebayashi *et al.*[10)] reported that ductile–brittle transition temperature in tempered martensitic steels decreased with decreasing the size of prior austenite grain. Gourgues *et al.*[11)] pointed out the importance of crystallography of boundaries for the cleavage crack propagation and reported that the "crystallographic packet" which was surrounded by high-angle boundaries was a unit controlling cleavage fracture behavior in a low-carbon bainitic steel. Morris *et al.*[12–15)] also proposed that the variant boundaries with large mis-

* Corresponding author: E-mail: SHIBATA.Akinobu@nims.go.jp

orientation of {001} cleavage planes would be effective for retarding cleavage fracture in martensitic steels. Recently we studied cleavage crack propagation behavior in a low-carbon martensitic steel by crystallographic orientation analysis and found that the cleavage crack propagation was arrested at the variant boundaries whose misorientation angles of {001} planes are large.[16] This findings strongly support the ideas proposed by Gourgues *et al.*[11] and Morris *et al.*[12–15]

Assuming that martensite or bainite holds Kurdjumov–Sachs (K-S) orientation relationship with respect to parent austenite phase ($\{111\}_\gamma//\{011\}_{\alpha'}$, $<\text{-}101>_\gamma//<\text{-}1\text{-}11>_{\alpha'}$ (subscripts $\gamma$ and $\alpha'$ indicate austenite and martensite (or bainite), respectively)), there are 24 crystallographic variants that can transform from a single austenite grain. From a crystallographic point of view, a block corresponds to single variant, and a packet consists of variants with the same parallel plane relationship. On the other hand, it is well known that the primitive step of martensitic/bainitic transformation involves lattice change from face-centered cubic (fcc) to body-centered cubic (bcc), which is accomplished by Bain deformation.[17] In Bain deformation, fcc lattice is compressed along one <001> direction and elongated along the other two <001> directions, and then transforms to bcc lattice. Because there are three kinds of Bain deformation (compression direction: $[001]_\gamma//[001]_{\alpha'}$, $[010]_\gamma//[001]_{\alpha'}$, $[100]_\gamma//[001]_{\alpha'}$), the 24 K-S variants can be divided into three groups. The variants belonging to an identical Bain deformation group have relatively small misorientation of {001} planes to each other.[16–19] Because the variant boundaries with large misorientation of {001} planes can arrest cleavage crack propagation,[16] it is expected that the aggregation of variants belonging to the same Bain deformation group (hereinafter, "Bain unit") has a great influence on low-temperature embrittlement. Takayama *et al.*[18] studied the effect of transformation temperature on the variant paring tendency in a low-carbon bainitic steel and reported that the variants belonging to the same Bain deformation group tended to form adjacently when the transformation temperature was high. Their results indicated that Bain unit size can be controlled by changing transformation temperature in bainitic steels. The present study prepared the martensite and bainite with various sizes of Bain unit by controlling transformation temperature and investigated the effect of Bain unit size on low-temperature fracture behavior in medium-carbon martensitic and bainitic steels.

## 2. Experimental Procedure

A medium-carbon steel (Fe-2Mn-0.4C (wt.%)) was used in the present study. The detailed chemical composition of the steel (in mass%) was C: 0.394, Si: 0.01, Mn: 1.97, P: <0.003, S: 0.0008, Al: 0.01, N: 0.0023, O: 0.0021, and Fe: balance. The homogenized sheets were austenitized at 1 000°C for 300 s, followed by water-quenching and sub-zero cooling in liquid nitrogen to obtain a fully martensitic structure. For obtaining bainite structures with various Bain unit sizes, the homogenized sheets were austenitized at 1 000°C for 300 s and then held at the temperature ranging from 350°C to 475°C for 600 s, followed by water-quenching and sub-zero cooling in liquid nitrogen.

Single-notched bending specimens were machined from the heat-treated specimens by spark wire cutting. The dimensions of the single-notched bending specimens were 1 mm × 3 mm × 20 mm with a notch depth of 1.5 mm and a notch radius of 0.15 mm. Three-point bending tests with a support span of 12 mm were conducted at a displacement rate of 0.5 mm $min^{-1}$ at liquid nitrogen temperature (−196°C). From the load–displacement curve of the three-point bending test, fracture toughness, $K_A$, was evaluated using the following equation:[20,21]

$$K_A = \frac{P_{max}}{B\sqrt{W}} f\left(\frac{a}{W}\right) \quad \text{..... (1)}$$

$$f\left(\frac{a}{W}\right) = \frac{3\frac{S}{W}\sqrt{\frac{a}{W}}}{2\left(1+2\frac{a}{W}\right)\left(1-\frac{a}{W}\right)^{3/2}}\left[1.99-\frac{a}{W}\left(1-\frac{a}{W}\right)\left\{2.15-3.93\left(\frac{a}{W}\right)+2.7\left(\frac{a}{W}\right)^2\right\}\right] \quad \text{..... (2)}$$

where $P_{max}$ is a maximum load in the load-displacement curve, $B$ is a specimen thickness (1 mm), $W$ is a specimen width (3 mm), $S$ is a support span (12 mm), and $a$ is a notch length (1.5 mm). At least two tests were performed for each of the specimens. Because the specimen thickness is 1 mm and not enough for satisfying small scale yielding condition, $K_A$ is not a valid plane strain fracture toughness but an apparent fracture toughness. Moreover, finite element (FE) simulations were carried out using the commercial Z-set code[22] to evaluate the local stress-intensity factor for the three-point bending test.

Microstructures of the specimens were characterized by scanning electron microscopy (SEM, JEOL: JSM-7800F) and electron backscattering diffraction (EBSD) using SEM (JEOL: JSM-7100F) after electrolytic polishing in a solution of 900 mL $CH_3COOH$ + 100 mL $HClO_4$. The EBSD measurements and analyses were performed with the TSL OIM Data Collection program and the TSL OIM Analysis program, respectively.

## 3. Results

### 3.1. Microstructure

**Figure 1** shows SEM images of (a) the as-quenched martensite and (b–f) the bainites formed at (b) 350°C, (c) 380°C, (d) 400°C, (e) 420°C, (f) 475°C. The as-quenched martensite contains almost no carbide (Fig. 1(a)), while a large number of carbides can be observed in the bainites (Figs. 1(b)–1(f)). We confirmed that there was no pro-eutectoid ferrite in all the specimens. The EBSD orientation maps and Bain maps of the specimens are presented in **Fig. 2**, where the high-angle boundaries with misorientation larger than 15° are drawn in the black lines. The colors in the EBSD orientation maps (Figs. 2(a)–2(f)) express the orientations parallel to the normal direction of the observed section. In the Bain maps (Figs. 2(g)–2(l)), on the other hand, the aggregations of martensite/bainite belonging to the same Bain deformation group are represented by the same colors (red, yellow, and blue, respectively). The mean Bain unit size with standard deviation of the as-quenched martensite, bainites formed at 350°C, 380°C, 400°C, 420°C, and 475°C, measured by line interception method, are 2.5 ± 0.6 $\mu$m, 2.1 ± 0.7 $\mu$m, 4.4 ± 1.4 $\mu$m,

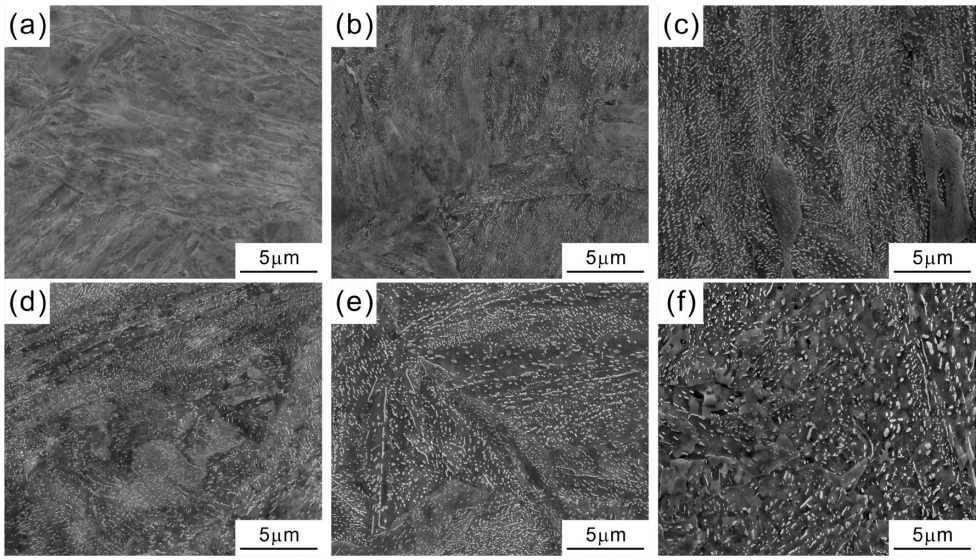


**Fig. 1.** SEM images of (a) the as-quenched martensite and (b–f) the bainites formed at (b) 350°C, (c) 380°C, (d) 400°C, (e) 420°C, (f) 475°C.

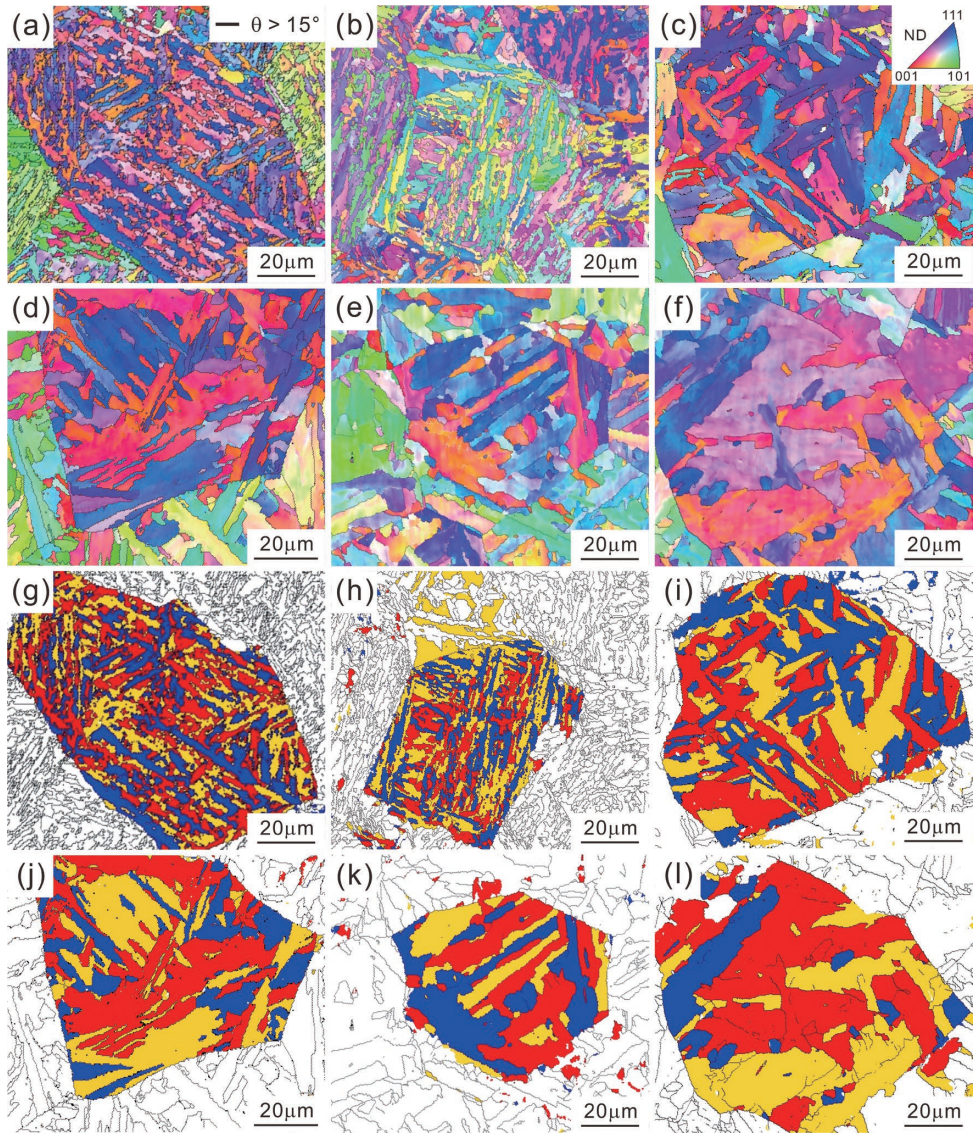


**Fig. 2.** EBSD orientation maps and Bain maps of the specimens; (a, g) the as-quenched martensite and the bainites formed at (b, h) 350°C, (c, i) 380°C, (d, j) 400°C, (e, k) 420°C, (f, l) 475°C. The high-angle boundaries with misorientation larger than 15° are drawn in the black lines. The colors in the EBSD orientation maps express the orientations parallel to the normal direction of the observed section. In the Bain maps, the aggregations of martensite/bainite belonging to the same Bain deformation group are represented by the same colors (red, yellow, and blue, respectively).

5.5 ± 2.3 $\mu$m, 6.9 ± 2.5 $\mu$m, and 16.2 ± 8.0 $\mu$m, respectively. **Figure 3** summarizes the change in the mean Bain unit size with formation temperature. As reported previously,[18] we can find the clear tendency that the Bain unit size of bainite decreases with decreasing the transformation temperature. In addition, the Bain unit size of the bainite formed at 350°C is slightly smaller than that of the as-quenched martensite.

### 3.2. Fracture Toughness Property

The load–displacement curves of the three-point bending tests at −196°C are presented in **Fig. 4**. The bainite formed at 350°C exhibited plastic deformation to some extent before the fracture. In contrast, the as-quenched martensite and the other bainites were fractured within the elastic strain regimes. The apparent fracture toughness evaluated from the load–displacement curves according to Eqs. (1) and (2) is

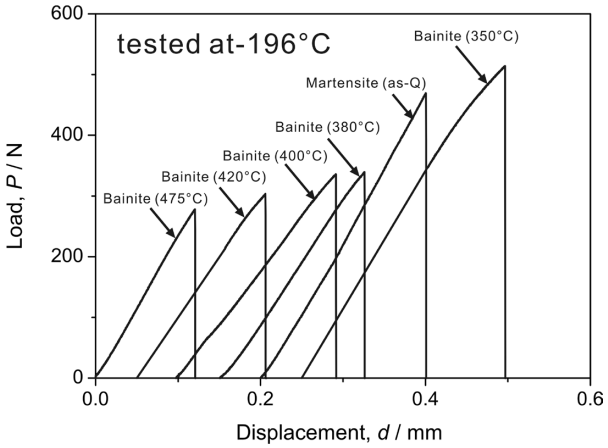


**Fig. 4.** Load–displacement curves of the three-point bending tests at −196°C.

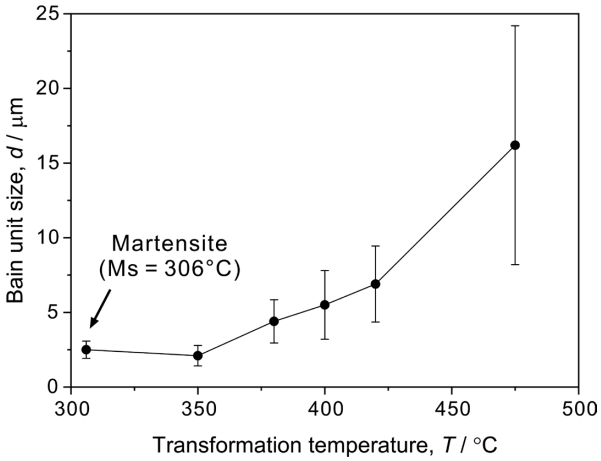


**Fig. 3.** Change in the mean Bain unit size with formation temperature.

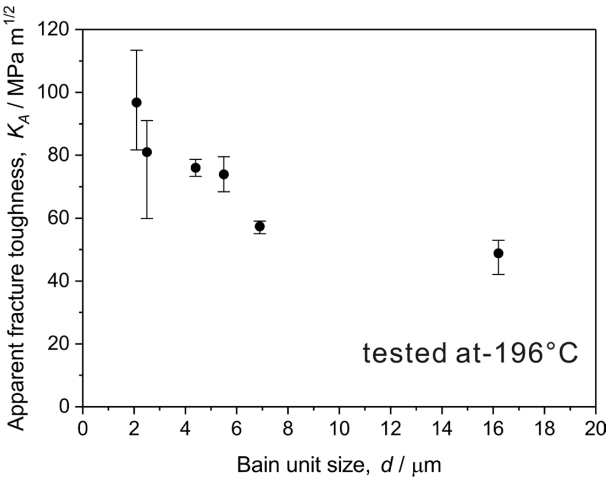


**Fig. 5.** Apparent fracture toughness of the specimens summarized as a function of the mean Bain unit size.

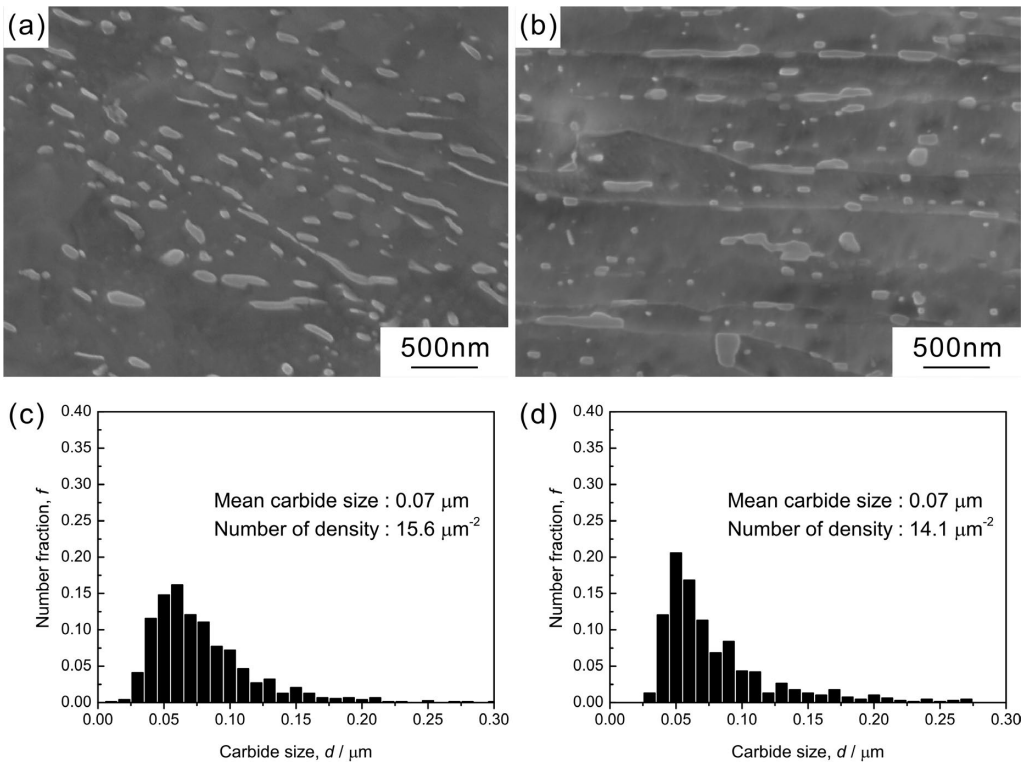


**Fig. 6.** (a, b) SEM images of (a) the tempered martensite and (b) the bainite formed at 475°C. (c, d) The distribution of carbide size in (c) the tempered martensite and (d) the bainite formed at 475°C.

summarized in **Fig. 5** as a function of the mean Bain unit size. We can find that the fracture toughness of martensite/bainite increases with decreasing the Bain unit size. This indicates that refinement of Bain unit size is an effective way to increase fracture toughness at low temperature.

As shown in Figs. 1 and 2, the microstructures of as-quenched martensite and bainites formed at different temperature differ not only Bain unit size but also carbide fraction. It is well known that carbide acts as an initiation site of brittle fracture and has a large influence on the fracture toughness. As a result, there is a possibility that the change in fracture toughness confirmed in Fig. 5 was not only attributed to the change in Bain unit size. In order to examine effects of both of Bain unit size and carbide distribution on fracture toughness, we compared the fracture toughness of the tempered martensite and the bainite formed at 475°C. For obtaining the tempered martensite with carbide distribution similar to the bainite formed at 475°C, the as-quenched martensite was tempered at 575°C for 7.2 ks. **Figures 6**(a) and 6(b) show SEM images of the tempered martensite (575°C) and the bainite formed at 475°C, respectively. Both the microstructures contain a large number of carbides mainly along the lath boundaries. The distributions of carbide size in the tempered martensite and the bainite formed at 475°C were measured from SEM images. As summarized in Figs. 6(c) and 6(d), the size and number density of carbides in the two specimens were almost the same. In addition, we confirmed that the tensile properties of two specimens were almost the same, though they were measured at room temperature (yield strength: 651 MPa, tensile strength: 782 MPa for the tempered martensite, and yield strength: 612 MPa, tensile strength: 806 MPa for the bainite formed at 475°C). **Figure 7** shows load–displacement curves of the three-point bending tests at −196°C for the tempered martensite and the bainite formed at 475°C. Although the bainite formed at 475°C was fractured within the elastic strain regime, the tempered martensite exhibited large plastic deformation. The apparent fracture toughness of the tempered martensite is 83.6 MPa $m^{1/2}$, much larger than that of the bainite formed at 475°C (48.8 MPa $m^{1/2}$). Because Bain unit size did not change by tempering, the Bain unit size of the tempered martensite was the same as the as-quenched martensite, *i.e.*, 2.5 $\mu$m. As a result, we can conclude that the improvement of fracture toughness at −196°C confirmed in Fig. 5 was attributed to the decrease in Bain unit size.

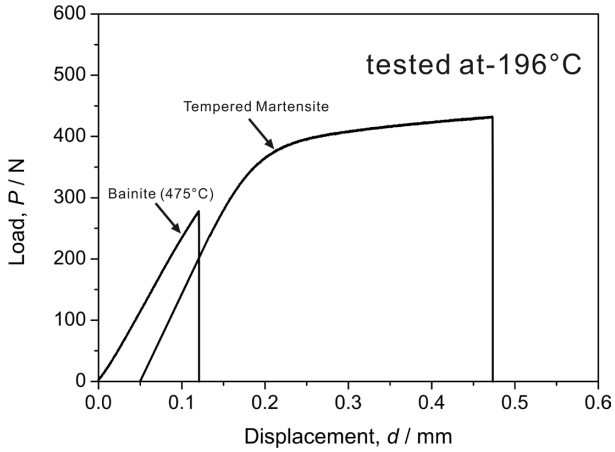


**Fig. 7.** Load–displacement curves of the three-point bending tests at −196°C for the tempered martensite and the bainite formed at 475°C.

## 4. Discussion

As shown in Figs. 5 and 7, the decrease in Bain unit size improved fracture toughness at lower temperature. According to the previous works,[2,23,24] low-temperature brittle fracture of martensite/bainite can be divided into three stages as schematically illustrated in **Fig. 8**. In Stage I, a micro-crack is initiated at carbide by either carbide/matrix decohesion or brittle fracture of carbide itself. In Stage II, the micro-crack propagates into the matrix across the carbide/matrix boundary and reaches the first "strong" matrix/matrix boundary. Then, in Stage III, the micro-crack penetrates the matrix/matrix boundary, leading to the final and unstable fracture. All of the bainites investigated in the present study contained carbides which could act as initiation sites of brittle fracture. In contrast, carbides could not be confirmed in the as-quenched martensite as shown in the SEM image of Fig. 1(a). However, we can assume that a certain amount of carbides also existed in the as-quenched martensite due to auto-tempering.[7] Thus, it can be considered that the effect of Bain unit size on the fracture of Stage I and Stage II is not large. Because the fracture toughness strongly depended on the Bain unit size as shown in Fig. 5, the "strong" matrix/matrix boundary corresponds to Bain unit boundary in mar-

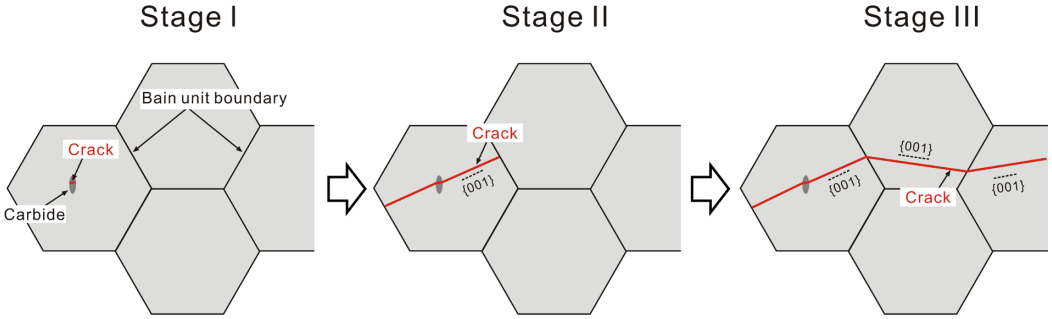


**Fig. 8.** Schematic illustration showing the cleavage crack propagation behavior. Stage I: a micro-crack is initiated at carbide by either carbide/matrix decohesion or brittle fracture of carbide itself. Stage II: the micro-crack propagates into the matrix across the carbide/matrix boundary and reaches the first "strong" matrix/matrix boundary. Stage III: the micro-crack penetrates the matrix/matrix boundary, leading to the final and unstable fracture. (Online version in color.)

tensite/bainite structure. We can consider that the Bain unit size would affect the brittle fracture process of transition from Stage II to Stage III.

**Figure 9** shows (a, c, d) SEM images and (b) a Bain map taken at areas approximately 100 $\mu$m away from the notch root of the specimens whose three-point bending tests were stopped just after reaching 80% of the fracture load; (a, b) the as-quenched martensite and (c, d) the bainite formed at 475°C. For the as-quenched martensite (Figs. 9(a) and 9(b)), several micro-cracks parallel to {001} cleavage planes formed around the notch root. These cracks stopped at the Bain unit boundaries, indicating that the crack propagation was arrested by the Bain unit boundaries. As shown in Figs. 9(c) and 9(d), the micro-cracks inside the carbide and the carbide/matrix interface can be observed in the bainite formed at 475°C. We observed in a wide area carefully, but could not find any micro-cracks that stopped at Bain unit boundaries in the bainite formed at 475°C. This observation results suggest that the Bain unit boundaries could not act as obstacles for crack propagation when the Bain unit size was notably large (16.2 $\mu$m).

In the following, we discuss the role of Bain unit boundary on brittle fracture based on fracture mechanics. At Stage II of fracture process shown in Fig. 8, the length of micro-crack formed around the notch root corresponds to the Bain unit size. The existence of such the micro-cracks was confirmed in Figs. 9(a) and 9(b). We can consider that a micro-crack, which penetrates Bain unit boundary, leads to the final rupture, when the local stress-intensity factor of the micro-crack exceeds a certain critical value ($K_{C\text{-}Local}$). Assuming that the micro-crack formed around the notch root exhibits a penny shape whose longitudinal length corresponds to the Bain unit size, the local stress-intensity factor of the micro-crack ($K_{Local}$) can be expressed as;[25,26]

$$K_{Local} = \frac{\sqrt{2}}{\pi}\sigma\sqrt{\pi a} \quad \text{..... (3)}$$

where $\sigma$ is a remote tensile stress and $a$ is a crack length (equal to the Bain unit size). Because the $K_{Local}$ decreases with decreasing the Bain unit size (length of micro-crack) according to Eq. (3), the tensile stress (*i.e.*, applied load) necessary to reach the critical value of local stress-intensity factor ($K_{C\text{-}Local}$) increases with decreasing the Bain unit size. Accordingly, the decrease in Bain unit size increased maximum load in the three-point bending test, resulting in the increasing of the apparent fracture toughness as confirmed in Fig. 5.

By FE simulations using Z-set code, we evaluated the critical value of local stress-intensity factor necessary for crack propagation across Bain unit boundary when the Bain unit size was below 6.9 $\mu$m. In the case when the Bain unit size was 16.2 $\mu$m, the Bain unit boundaries could not prevent crack propagations as shown in Figs. 9(c) and 9(d). In order to evaluate the critical value of local stress-intensity factor, we made the following two assumptions;

(i) The micro-crack forms 100 $\mu$m ahead of the notch root at the mid-thickness section of the three-point bending specimen. The crack is penny-shaped whose broad face is parallel to the notch and longitudinal length of the crack is the same as the Bain unit size.

(ii) Strictly speaking, plastic deformation (even small amount) should be involved during the fracture process.

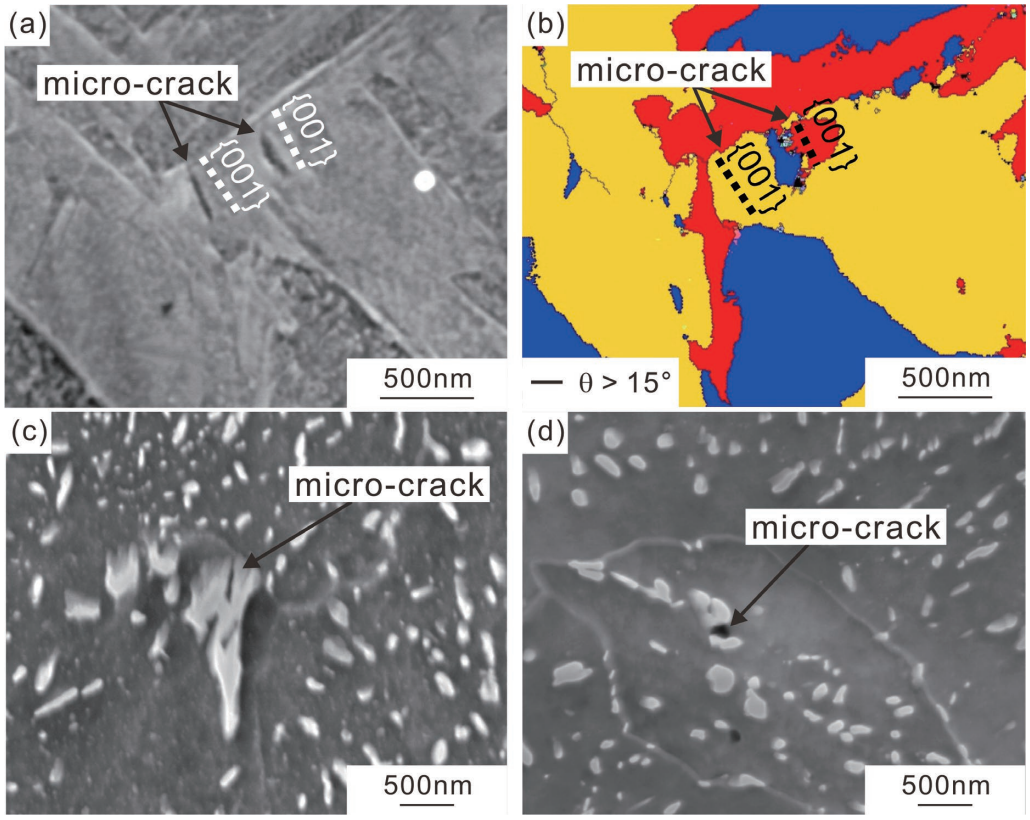


**Fig. 9.** (a, c, d) SEM images and (b) Bain map taken at areas approximately 100 $\mu$m away from the notch root of the specimens whose three-point bending tests were stopped just after reaching 80% of the fracture load; (a, b) the as-quenched martensite and (c, d) the bainite formed at 475°C.

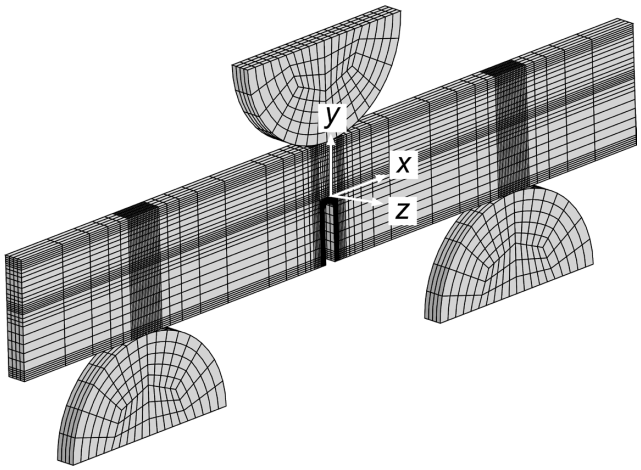


**Fig. 10.** Three-dimensional FE mesh for one half of the three-point bending specimen.

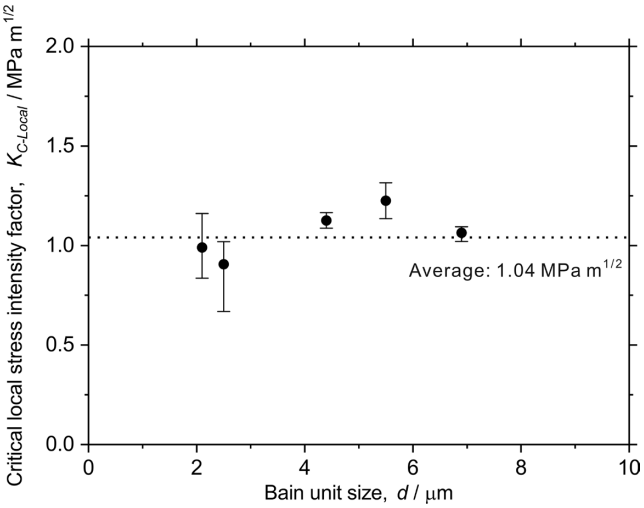


**Fig. 11.** Critical local stress-intensity factor plotted as a function of Bain unit size.

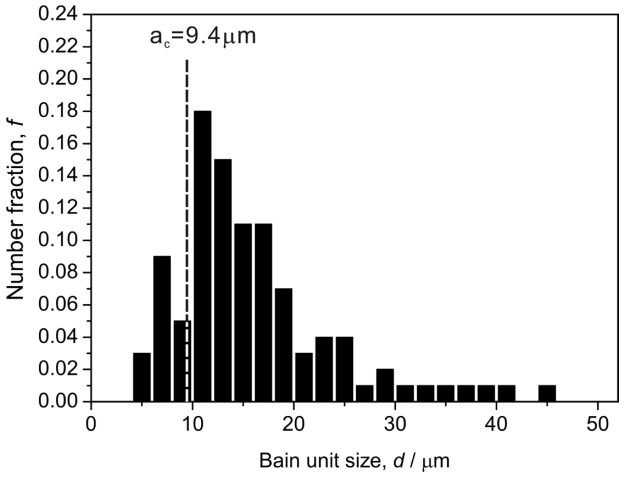


**Fig. 12.** Bain unit size distribution of the bainite formed at 475°C.

However, we simply assume that a mode I fracture occurs, and any plastic deformation does not occur before fracture. Because the final ruptures occurred without obvious macroscopic plastic deformations as shown in the load-displacement curves (Fig. 4), we can consider that the FE simulation results using elastic continuum body (Young's Modulus: 200 GPa, Poisson ratio: 0.3) do not differ so much from the actual behavior.

As shown in **Fig. 10**, we used three-dimensional FE mesh for one half of the three-point bending specimen and set the boundary condition that $U_z$ (displacement along $Z$ direction) = 0 at $z$ = 0. Then the $\sigma_{xx}$ (at $x$ = 0 $\mu$m, $y$ = 100 $\mu$m, $z$ = 0 $\mu$m) was computed under the situation that the applied load became the maximum load of the three-point bending test, because we simply assumed that the micro-crack forms 100 $\mu$m ahead of the notch root at the mid-thickness section of the specimen as described above. The critical local stress-intensity factor can be obtained by substituting the $\sigma_{xx}$ for $\sigma$ and the Bain unit size for $a$ to Eq. (3). As summarized in **Fig. 11**, the critical local stress-intensity factor does not significantly change with Bain unit size, and the average value is 1.04 MPa m$^{1/2}$.

As described above, we can consider that Bain unit boundaries could not act as obstacles for crack propagation for the bainite formed at 475°C (Bain unit size: 16.2 $\mu$m). This suggests that the propagation of micro-crack across matrix/carbide boundary (transition from Stage I to Stage II in Fig. 8) suddenly led to final rupture. Thus, the apparent fracture toughness of bainite formed at 475°C corresponds to the propagation of micro-crack across matrix/carbide boundary. By substituting the critical local stress-intensity factor of 1.04 MPa m$^{1/2}$ and maximum load in the load-displacement curve of bainite formed at 475°C to Eq. (3), the critical crack length below which crack stops at Bain unit boundary was estimated at 9.4 $\mu$m. That is, the Bain unit boundary whose interval is less than 9.4 $\mu$m can become obstacle for the crack propagation. This is consistent with the three-point bending tests that the fracture toughness of martensite/bainite with Bain unit size less than 6.9 $\mu$m notably changed depending on the Bain unit size. **Figure 12** shows a Bain unit size distribution of the bainite formed at 475°C. It can be found that almost all of the Bain unit size was larger than 9.4 $\mu$m. Therefore, we could not observe any micro-cracks that stopped at Bain unit boundary, and Bain unit boundary could not prevent crack propagation in the bainite formed at 475°C.

## 5. Conclusions

We investigated effect of Bain unit size on low-temperature fracture of medium-carbon martensitic and bainitic steels and reached the following conclusions.

(1) The martensite and bainite with Bain unit size ranging from 2.1 $\mu$m to 16.2 $\mu$m were prepared. The three-point bending tests revealed that the apparent fracture toughness increased with decreasing the Bain unit size. Moreover, the apparent fracture toughness of tempered martensite with Bain unit size of 2.5 $\mu$m was much higher than that of bainite with Bain unit size of 16.2 $\mu$m even when the carbide size and distribution were almost the same. Thus, we concluded that the decrease in Bain unit size improved the fracture toughness at low temperature.

(2) The micro-cracks were observed in the specimens of as-quenched martensite with Bain unit size of 2.5 $\mu$m and bainite formed at 475°C with Bain unit size of 16.2 $\mu$m whose three-point bending tests were stopped just after reaching 80% of the fracture load. For the as-quenched

martensite, there were several micro-cracks stopped at the Bain unit boundaries. In contrast, we could not observe any micro-cracks of which length corresponded to the Bain unit size in the bainite formed at 475°C. When the Bain unit size was large, final unstable fracture occurred just after propagation of crack at matrix/carbide boundaries. With decreasing the Bain unit size, on the other hand, the micro-crack stopped at the Bain unit boundaries. The additional load was necessary for further propagation of crack which stopped at the Bain unit boundaries, leading to the improvement of fracture toughness.

(3) The critical local fracture toughness corresponding to the propagation of crack across the Bain unit boundaries was estimated at 1.04 MPa $m^{1/2}$ by FE simulations. By using this value, we found that the Bain unit boundary whose interval was less than 9.4 $\mu$m could become obstacle for the crack propagation after penetrating matrix/carbide boundary. Almost all of the interval of Bain unit boundary in the bainite formed at 475°C were more than 9.4 $\mu$m, resulting in that Bain unit boundary could not stop crack propagation.

**Acknowledgement**

This study was financially supported by JSPS KAKENHI (Grant Numbers JP19H02459 and JP20K21083).

## REFERENCES

1) R. O. Ritchie and J. F. Knott: *J. Mech. Phys. Sol.*, **21** (1973), 395. https://doi.org/10.1016/0022-5096(73)90008-2
2) A. Pineau, A. A. Benzerga and T. Pardoen: *Acta Mater.*, **107** (2016), 424. https://doi.org/10.1016/j.actamat.2015.12.034
3) A. R. Marder and G. Krauss: *Trans. ASM*, **60** (1967), 651.
4) J. M. Marder and A. R. Marder: *Trans. ASM*, **62** (1969), 1.
5) S. Morito, H. Tanaka, R. Konishi, T. Furuhara and T. Maki: *Acta Mater.*, **51** (2003), 1789. https://doi.org/10.1016/s1359-6454(02)00577-3
6) S. Morito, X. Huang, T. Furuhara, T. Maki and N. Hansen: *Acta Mater.*, **54** (2006), 5323. https://doi.org/10.1016/j.actamat.2006.07.009
7) A. Shibata, G. Miyamoto, S. Morito, A. Nakamura, T. Moronaga, H. Kitano, I. Gutierrez-Urrutia, T. Hara and K. Tsuzaki: *Acta Mater.*, **246** (2023), 118675. https://doi.org/10.1016/j.actamat.2023.118675
8) S. Matsuda, T. Inoue, H. Mimura and Y. Okamura: Proc. of Int. Sympo. on Toward Improved Ductility and Toughness, (1971), 45.
9) C. Wang, M. Wang, J. Shi, W. Hui and H. Dong: *Scripta Mater.*, **58** (2008), 492. https://doi.org/10.1016/j.scriptamat.2007.10.053
10) S. Takebayashi, K. Ushioda, N. Yoshinaga and S. Ogata: *Mater. Trans.*, **54** (2013), 1110. https://doi.org/10.2320/matertrans.M2013079
11) A. F. Gourgues, H. M. Flower and T. C. Lindley: *Mater. Sci. Technol.*, **16** (2000), 26. https://doi.org/10.1179/026708300773002636
12) J. W. Morris, Jr., C. S. Lee and Z. Guo: *ISIJ Int.*, **43** (2003), 410. https://doi.org/10.2355/isijinternational.43.410
13) J. W. Morris, Jr.: *ISIJ Int.*, **51** (2011), 1569. https://doi.org/10.2355/isijinternational.51.1569
14) J. W. Morris, C. Kinney, K. Pytlewski and Y. Adachi: *Sci. Technol. Adv. Mater.*, **14** (2013), 014208. https://doi.org/10.1088/1468-6996/14/1/014208
15) C. C. Kinney, K. R. Pytlewski, A. G. Khachaturyan and J. W. Morris: *Acta Mater.*, **69** (2014), 372. https://doi.org/10.1016/j.actamat.2014.01.058
16) M. Tsuboi, A. Shibata, D. Terada and N. Tsuji: *Metall. Mater. Trans. A*, **48A** (2017), 3261. https://doi.org/10.1007/s11661-017-4107-9
17) Z. Nishiyama: Martensitic Transformation, Academic Press, New York, (1978), 5.
18) N. Takayama, G. Miyamoto and T. Furuhara: *Acta Mater.*, **60** (2012), 2387. https://doi.org/10.1016/j.actamat.2011.12.018
19) D. Fukui, Y. Kawahito, N. Miyazawa and N. Nakada: *Mater. Charact.*, **191** (2022), 112157. https://doi.org/10.1016/j.matchar.2022.112157
20) T. L. Anderson: Fracture Mechanics, CRC Press, New York, (2017), 361.
21) ASTM E399-12, 2012.
22) Zset: http://www.zset-software.com. 2015
23) J. I. San Martin and J. M. Rodriguez-Ibabe: *Scripta Mater.*, **40** (1999), 459. https://doi.org/10.1016/S1359-6462(98)00467-9
24) A. Lambert-Perlade, A. F. Gourgues, J. Besson, T. Sturel and A. Pineau: *Metall. Mater. Trans. A*, **35A** (2004), 1039. https://doi.org/10.1007/s11661-004-1007-6
25) H. Tada, P. Paris and G. R. Irwin: The Stress Analysis of Cracks Handbook, 3rd ed., ASME Press, New York, (2000), 342.
26) T. L. Anderson: Fracture Mechanics, 4th ed., CRC Press, New York, (2017), 50.